中國機械工程學刊第四十一卷第二期第221~228頁(民國一百零九年)
Journal of the Chinese Society of Mechanical Engineers, Vol.41, No.2, pp 221~228 (2020)

An Evaluation of Spatial and Spherical Motion Generation for Application in Knee Motion Analysis and Simulation

Wen-Tzong Lee

Keywords: Knee Motion, Tibial-femoral Motion, Spatial Linkage, Spherical Linkage, Motion Generation.

ABSTRACT

In terms of a mechanical description, the human knee has typically been represented using the open-loop Cylindrical-Cylindrical-Cylindrical linkage. This linkage has a maximum of 6 degrees of freedom. While this linkage has the capacity to exhibit natural knee motion precisely, it requires the user to define up to 6 independent motion parameter ranges to achieve it. In comparison, achieving natural human knee motion using a single degree of freedom linkage could be a significant improvement since the user is required to define only a single motion parameter range. In this work, the applicability of the spatial Revolute-Revolute-Spherical-Spherical and Four Revolute Spherical linkages (both spatial four-bar linkages having single degrees of freedom) for human knee motion analysis and simulation are evaluated. Optimization models for the motion generation of both linkages are applied to produce linkage dimensions that achieve natural knee motion. As an example, the dimensions of Revolute-Revolute-Spherical-Spherical and Four Revolute Spherical linkages are calculated to achieve a group of tibial-femoral positions over an average walking cycle. These linkages are then modeled and their motion simulated in a CAD-based mechanical modeling environment.

INTRODUCTION

Conventional Linkage Representation of the Human Knee

As engineers began to provide mechanical descriptions to joints in the human body, studies were being presented to help describe human joint motion in three dimensions. In 1983, tibial and femoral coordinate systems and a coordinate system transformation method were presented to facilitate communication between engineers and surgeons (Grood and Suntay 1983). The coordinate systems presented in this 1983 work for the tibia and femur are illustrated in Figure 1a. The Z-axis for both bones was oriented on the mechanical axis of the femur. The mechanical axis is defined as a line that connects the centers of geometric features of the respective bones.

The origin of each coordinate system is located at the center points used in the creation of the mechanical axis. Figure 1b includes the identification of the signs for the rotations and translations along with a linkage illustration showing how to position one bone with respect to the other. By starting with general transformation descriptions between two objects, a method for describing the kinematics of the femur and tibia in three-dimensional space was produced (Grood and Suntay 1983). As a result, the characterization of human knee motion can be described by three principle rotations and translations (enabling the accurate display of complex knee motion). As illustrated in Figure 1b, this motion can be achieved by an open-loop Cylindrical-Cylindrical-Cylindrical (or CCC) linkage where each cylindrical joint achieves an in-plane knee rotation and an orthogonal-to-plane knee translation (thus utilizing up to 6 degrees of freedom).

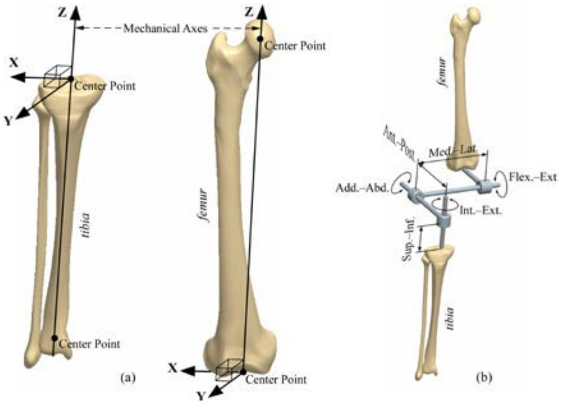

Fig. 1. (a) Tibia and femur coordinate systems and (b) open-loop CCC linkage with tibiofemoral motion references

Paper Received August, 2019. Revised October, 2019, Accepted February, 2020, Author for Correspondence: Wen-Tzong Lee.

Department of Biomechatronics Engineering, National Pingtung University of Science and Technology, Pingtung, 91201, Taiwan.

Current Challenges in In Vivo and In Vitro Human Knee Motion Analysis and Simulation

The most common in vivo setting for human motion analysis is in a *gait lab*, where the subjects are instrumented with reflective markers (applied to the skin) to track human motion. The chief complication with this approach lies in the skin and underlying soft tissue not being rigidly-fixed to the underlying bones (Benoit et al. 2007). While general human motion can be measured through skin markers, measuring the exact spatial motion of individual bones is difficult. Further, the already imprecise human motion data (recorded using skin markers) is made even more imprecise by representing it in a single plane where general knee motion traits such as external rotation, translation and varus-valgus movement are not captured (Dennis et al. 2005). Subsequently, it is impossible to obtain a complete and accurate three-dimensional assessment of knee motion using data that is recorded from external skin-based markers and expressed in planar space.

The limitations of the noted in vivo knee motion measurement approach are not encountered in cadaver-based in vitro testing. Here, a direct marker-to-bone connection (rather than marker-to-skin connection) is utilized-eliminating the bone position error introduced by the motion of skin and muscle tissue. Because an in vitro leg specimen is used, a system of mechanical linkages, pulleys and cables are employed to artificially support and actuate the leg through flexion and extension (Belvedere et al. 2012). While in vitro testing provides greater tibiofemoral motion accuracy, artificially actuating a cadaveric leg could introduce constraints that would not exist under natural, living muscle and tendon-based leg actuation (therefore introducing error in artificial-actuated tibiofemoral motion).

Spatial Four-bar Linkages and Motion Generation

Planar linkages are restricted to motion in 2-dimensional space. Common examples of planar linkages include the *planar four-bar* linkage and the *slider-crank* linkage. In comparison, *spatial* linkages can exhibit motion in 3-dimensional space. Two types of spatial linkages are considered in this work due to their simple design and spatial kinematics: the *Revolute-Revolute-Spherical-Spherical* (or RRSS) and the *Four Revolute Spherical* (or 4R Spherical) linkages. The RRSS linkage (Figure 2a) is a four-bar spatial linkage where the driving link is bounded by two revolute joints and the follower link is bounded by two spherical joints. The 4R Spherical linkage (Figure 2b) is a four-bar spatial linkage where all links are bounded by two revolute joints and these joints are oriented so that their axes all continually intersect at a common point-the center of the linkage sphere (Lee and Russell 2007). This common point of joint axis intersection constrains the spatial motion of the 4R Spherical linkage to a spherical surface. The RRSS linkage has 2 degrees of freedom (although 1 degree of freedom, the rotation of the follower link about its center axis lengthwise, has no effect on its overall kinematics) and the 4R Spherical linkage has a single degree of freedom.

The objective in four-bar linkage *motion generation* (a type of inverse problem in kinematics) is to calculate the linkage dimensions required to approximate a group of prescribed coupler link positions (Lee and Russell 2018). In 2013, optimization models were presented for both RRSS and 4R Spherical linkage motion generation (Russell and Shen 2013). With these models, the dimensions for defect-free RRSS and 4R Spherical linkages that approximate a group of prescribed spatial coupler link positions are calculated. In this work, the prescribed positions are tibial positions achieved over the human gait cycle for an average specimen (Benoit et al. 2007).

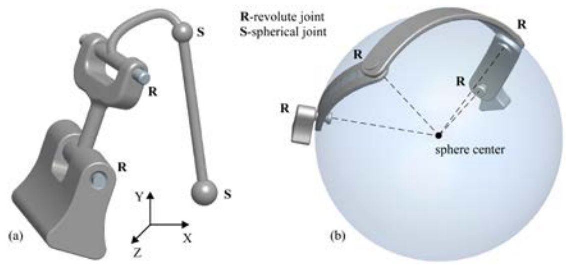

Fig. 2. (a) RRSS and (b) 4R Spherical linkages

Objective and Motivation of Work

Due to the noted challenges associated with in vivo and in vitro human knee motion analyses and the level of involvement in prescribing knee motion using the 6-DOF open-loop CCC linkage, this work examines the potential of spatial RRSS and 4R Spherical motion generation in achieving natural knee motion. As an example, the dimensions both linkage types are calculated to achieve a group of tibial-femoral positions taken over an average walking cycle. These linkages are then modeled and knee motion simulated with them in a CAD-based mechanical modeling environment. This work is intended to supplement existing knee analysis methods by providing a means to conduct basic, but realistic leg motion analyses in a CAD-based mechanical modeling environment.

TIBIOFEMORAL MOTION DURING GAIT

While human knee motion is comprised of various daily-living activities (e.g., squatting, climbing and descending stairs and kneeling), the most common activity associated with knee motion is level-plane walking or *gait*. Researchers have divided the human gait cycle into two phases; the *stance phase* and the *swing* phase of gait (Gage et al. 1995). Because humans are bipedal, one leg is grounded while the other is in travel in a gate cycle. Also, because knee is loaded during the stance phase, data is typically reported for this phase. In 1995, the tibiofemoral motion of subjects during gait was presented (Benoit et al. 2007). While the primary purpose of this 1995 work was to determine the accuracy of skin-based markers, it also provided in vivo tibiofemoral motion data for the femoral and tibial bones during the gait cycle. Figure 3 includes a graphical representation of this data averaged while a tabular representation (at 0, 25, 50, 75 and 100% of the stance phase) is included in Table 1.

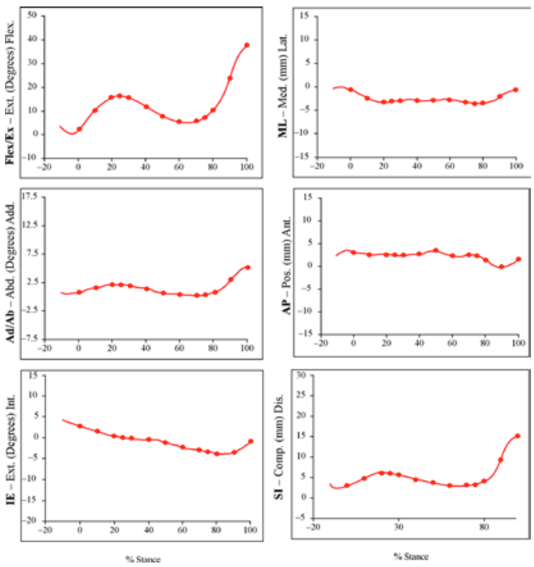

Fig. 3. Average human knee motion rotation and translation plots during gait

Table 1 Average human knee translations and rotations during gait

% Stance Phase	Flex/Ex [deg.]	IE [deg.]	Ad/Ab [deg.]	AP [mm]	ML [mm]	SI [mm]
0	2.40	2.92	0.85	3.25	−0.68	2.45
25	16.81	−0.03	2.15	2.58	−3.16	5.81
50	7.75	−1.27	0.58	3.35	−2.99	3.50
75	7.68	−3.35	0.32	2.41	−3.60	3.20
100	36.92	−1.30	5.02	1.45	−0.76	15.05

EXAMPLES

Tibiofemoral Motion Tracking

Given the displacement relationships of the femur and tibia during gait in Section 2, the precise spatial positions of the femur and tibia during the gait cycle were measured. Figure 4 illustrates a 3-point position tracker rigidly-affixed to the CAD model of the femur. After defining the tibia and femur coordinate systems in Figure 1a and displacing the femur according to the Table 1 knee rotation and translation values, the coordinates of points **p**, **q** and **r** on the position tracker data were measured in spatial Cartesian form. Table 2 includes five femur positions with respect to the tibia. These positions represent the five stance phase instances in Table 1.

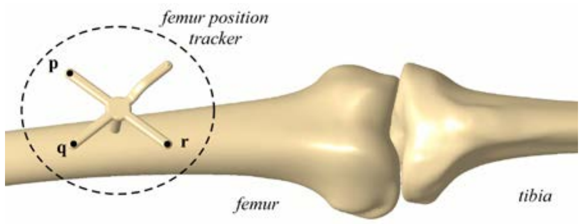

Fig. 4. CAD model of femur and tibia (including femur position tracker)

Table 2 Femur position tracker coordinates

% Stance Phase	**p** [mm]	**q** [mm]	**r** [mm]
0	−12.50, 55, 185.81	32.50, 55, 185.81	32.50, 55, 132.19
25	−12.45, 39.11, 191.12	32.44, 36.02, 191.18	32.84, 40.88, 137.78
50	−11.99, 38.45, 190.82	32.73, 33.53, 190.96	33.43, 38.38, 137.56
75	−10.61, 7.42, 197.24	34.34, 5.62, 196.26	33.75, 18.89, 144.31
100	−1.50,−63.77, 196.57	43.39,−64.35, 193.57	40.88,−33.28, 149.94

RRSS Motion Generation and Knee Motion Analysis and Simulation

Here, the dimensions for an RRSS linkage that approximates the femur position coordinates in Table 2 are calculated. Figure 5 includes the dimensions and link displacement angles for the RRSS linkage. The dimensions are the spatial Cartesian coordinates for joint locations $\mathbf{a}_0$, $\mathbf{a}_1$, $\mathbf{b}_0$, $\mathbf{b}_1$, the spatial coordinates for the revolute joint axis unit vectors $\mathbf{ua}_0$ and $\mathbf{ua}_1$. The link displacement angles are the *driving link* (link $\mathbf{a}_0 - \mathbf{a}_1$ in Figure 5) displacement angle θ and the *coupler link* (link $\mathbf{a}_1 - \mathbf{b}_1$ in Figure 5) displacement angle α. Figure 5 also includes dimensions $\mathbf{p}_1$, $\mathbf{q}_1$ and $\mathbf{r}_1$. These are the Cartesian coordinates measured from the femur position tracker (Figure 4), specifically, the coordinates given in Table 2 at the 0% stance phase. Because these coordinates are part of coupler link, they are illustrated affixed to this link.

Russell and Shen presented a constrained optimization model for the motion generation of RRSS linkages (Russell and Shen 2013). Given the coordinates for a group of prescribed positions and the initial values for each of the RRSS dimensions and link displacement angles, the optimization model calculates the optimum RRSS dimensions and link displacement angles. Table 3 includes the initial and calculated RRSS dimensions and link displacement angles using the RRSS motion generation model. This linkage is illustrated in Figure 6. Both the femur position coordinates achieved by the calculated RRSS linkage and the position error produced by this linkage is given in Tables 4 and 5 respectively. The position error in Table 5 is the scalar differences between the prescribed (Table 2) and achieved (Table 4) femur position coordinates. The 1.1mm *average error* in Table 5 is the sum of the scalar differences (excluding the zero differences for the 0% stance) divided by 36-the number of scalar differences.

To achieve femoral motion using the open loop C-C-C linkage (Figure 1b), the user must define values for each of its six degrees of freedom. In comparison, the femur positions in Table 4 is achieved by simply rotating the driving link (link $\mathbf{a}_0 - \mathbf{a}_1$ in Figure 6) of the RRSS linkage over the calculated driving link displacement angles (angles $\theta_2 \sim \theta_5$ in Table 3). Figure 7 illustrates a CAD model of the knee at 0% and 100% stance. In this model, the femur is affixed to the RRSS coupler link and the *ground link* (link $\mathbf{a}_0 - \mathbf{b}_0$ in Figure 6) is affixed to the tibia.

Figure 8 is a plot of the coupler displacement angle (α) versus the crank displacement angle (θ) over the given femoral motion range. This illustrates that the RRSS linkage is free of circuit defects (also called *singularities*) over the femoral motion range.

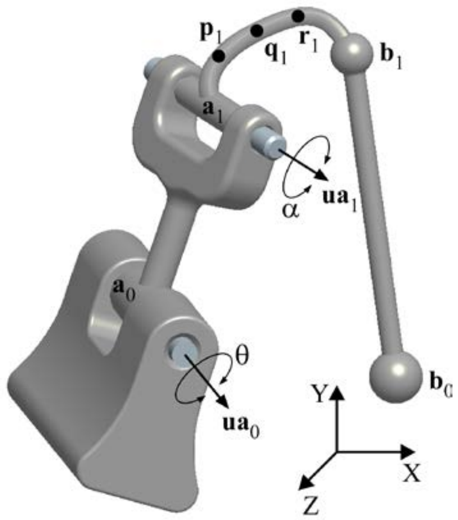

Fig. 5. RRSS linkage dimensions and link displacement angles

Table 3 Initial and calculated RRSS linkage dimensions and link displacement angles

dimension and unit	initial values	calculated values
$\mathbf{a}_0$ [mm]	7.71, 15.49,−6.55	7.49, 14.90,−7.24
$\mathbf{a}_1$ [mm]	7.86,−20.76, 10.09	8.34,−23.01, 6.68
$\mathbf{b}_0$ [mm]	−1.62,−14.11,−10.67	−2.02,−12.87,−10.27
$\mathbf{b}_1$[mm]	−12.18,−20.89, 9.60	−12.18,−16.55, 10.22
$\mathbf{ua}_0$ [no units]	1, 0, 0	0.76, 0.24, 0.61
$\mathbf{ua}_1$ [no units]	1, 0, 0	0.99,−0.03,−0.15
$\theta_2 \sim \theta_5$ [deg]	5, 5, 5, 5	1.01, 1.11, 2.77, 6.91
$\alpha_2 \sim \alpha_5$ [deg]	10, 10, 10, 10	4.77, 5.22, 12.75, 30.54

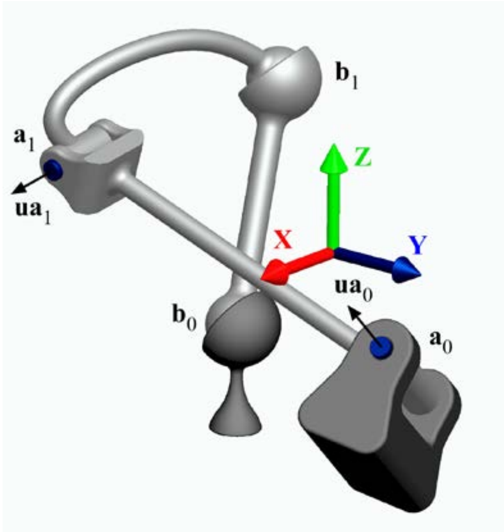

Fig. 6. Calculated RRSS linkage

Table 4 Femur position coordinates achieved by the calculated RRSS linkage

% Stance Phase	**p** [mm]	**q** [mm]	**r** [mm]
0	−12.50, 55, 185.81	32.50, 55, 185.81	32.50, 55, 132.19
25	−11.53, 37.39, 191.98	33.46 37.33, 191.88	33.35, 42.45, 138.50
50	−11.43, 35.71, 192.47	33.57, 35.64, 192.36	33.44, 41.24, 139.03
75	−9.40, 6.64, 198.51	35.591, 6.492, 198.11	35.17, 20.09, 146.24
100	−2.39,−63.93, 194.98	42.57,−64.05, 193.33	41.05,−33.02, 149.62

Table 5 Femur position errors produced by the calculated RRSS linkage (average error: 1.1mm)

% Stance Phase	**p** [mm]	**q** [mm]	**r** [mm]
0	0,0,0	0,0,0	0,0,0
25	0.92, 1.72, 0.86	1.03, 1.31, 0.70	0.51, 1.57, 0.72
50	0.56, 2.74, 1.66	0.83, 2.11, 1.40	0.01, 2.86, 1.47
75	1.20, 0.79, 1.28	1.25, 0.86, 1.85	1.42, 1.21, 1.94
100	0.89, 0.17, 1.59	0.82, 0.30, 0.25	0.17, 0.26, 0.32

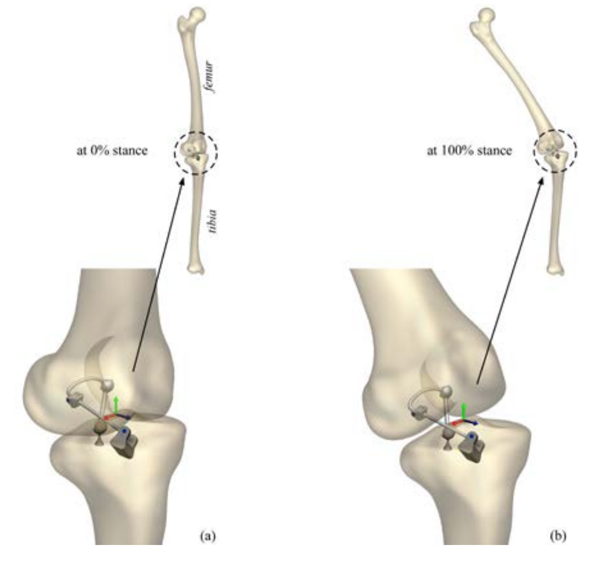

Fig. 7. Tibiofemoral motion with RRSS linkage at (a) 0% stance and (b) 100% stance

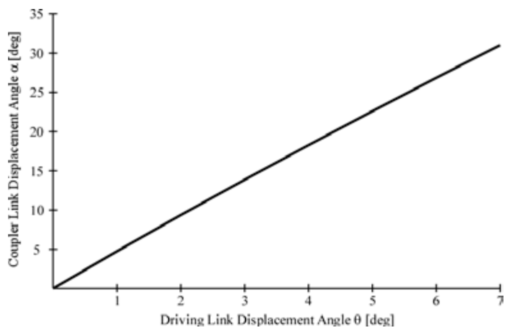

Fig. 8. RRSS coupler angular displacement (α) versus crank angular displacement (θ) over given femoral motion range

4R Spherical Motion Generation and Knee Motion Analysis and Simulation

Here, the dimensions for a 4R Spherical linkage that approximates the femur position coordinates in Table 2 are calculated. Figure 9 includes the dimensions and link displacement angles for the 4R Spherical linkage. Like the RRSS linkage, the dimensions are the spatial Cartesian coordinates for joint locations $\mathbf{a}_0$, $\mathbf{a}_1$, $\mathbf{b}_0$, $\mathbf{b}_1$, the spatial coordinates for the revolute joint axis unit vectors $\mathbf{ua}_0$ and $\mathbf{ua}_1$. The unit vectors $\mathbf{ua}_0$ and $\mathbf{ua}_1$ however are vectors from the sphere's origin (which is the coordinate system origin as illustrated in Figure 9) to joint locations $\mathbf{a}_0$ and $\mathbf{a}_1$ respectively. Therefore the unit vectors for the 4R Spherical linkage are $\mathbf{ua}_0 = \mathbf{a}_0 / |\mathbf{a}_0|$ and $\mathbf{ua}_1 = \mathbf{a}_1 / |\mathbf{a}_1|$. Like the RRSS linkage, the link displacement angles are the *driving link* (link $\mathbf{a}_0 - \mathbf{a}_1$ in Figure 9) displacement angle θ and the *coupler link* (link $\mathbf{a}_1 - \mathbf{b}_1$ in Figure 9) displacement angle α. Figure 9 also includes dimensions $\mathbf{p}_1$, $\mathbf{q}_1$ and $\mathbf{r}_1$- the coordinates measured from the femur position tracker given in Table 2 at the 0% stance phase.

Russell and Shen presented a constrained optimization model for the motion generation of 4R Spherical linkages (Russell and Shen 2013). Given the coordinates for a group of prescribed positions and the initial values for each of the 4R Spherical dimensions and link displacement angles, the optimization model calculates the optimum 4R Spherical dimensions and link displacement angles. Table 6 includes the initial and calculated 4R Spherical dimensions and link displacement angles using the 4R Spherical motion generation model. This linkage is illustrated in Figure 10. Both the femur position coordinates achieved by the calculated 4R Spherical linkage and the position error produced by this linkage is given in Tables 7 and 8 respectively. The position error in Table 8 is the scalar differences between the prescribed (Table 2) and achieved (Table 7) femur position coordinates. Like Table 5, the 2.5mm *average error* in Table 8 is the sum of the scalar differences (excluding the zero differences for the 0% stance) divided by 36-the number of scalar differences.

To achieve femoral motion using the open loop C-C-C linkage (Figure 1b), the user must define values for each of its six degrees of freedom. In comparison, the femur positions in Table 7 is achieved by simply rotating the driving link (link $\mathbf{a}_0 - \mathbf{a}_1$ in Figure 10) of the 4R Spherical linkage over the calculated driving link displacement angles (angles θ_2~θ_5 in Table 6). Figure 11 illustrates a CAD model of the knee at 0% and 100% stance. In this model, the femur is affixed to the 4R Spherical coupler link and the *ground link* (link $\mathbf{a}_0 - \mathbf{b}_0$ in Figure 10) is affixed to the tibia.

Figure 12 is a plot of the coupler displacement angle (α) versus the crank displacement angle (θ) over the given femoral motion range. Like Figure 8, Figure 12 illustrates that the 4R Spherical linkage is free of circuit defects over the femoral motion range.

Table 6 Initial and calculated 4R Spherical linkage dimensions and link displacement angles

dimension and unit	initial values	calculated values
$\mathbf{a}_0$ [mm]	1, 1, 1	0.66, 0.50, 0.56
$\mathbf{a}_1$ [mm]	1, 1, 1	0.93, 0.33, 0.17
$\mathbf{b}_0$ [mm]	1, 1, 1	0.98, 0.05, 0.17
$\mathbf{b}_1$[mm]	1, 1, 1	0.83,−0.14,−0.54
θ_2~θ_5 [deg]	10, 10, 10, 10	−6.83,−7.79,−14.33,−23.33
α_2~α_5 [deg]	10, 10, 10, 10	9.63, 11.21, 24.41, 52.86

Table 7 Femur position coordinates achieved by the calculated 4R Spherical linkage

% Stance Phase	**p** [mm]	**q** [mm]	**r** [mm]
0	−12.50, 55, 185.81	32.50, 55, 185.81	32.50, 55, 132.19
25	−12.50, 38.75, 189.87	32.46, 37.09, 190.21	33.03, 41.32, 136.76
50	−12.51, 35.75, 190.46	32.44, 33.90, 190.82	33.07, 38.93, 137.43
75	−12.22, 7.83, 193.57	32.70, 5.35, 193.62	33.45, 17.90, 141.49
100	−7.27,−59.97, 183.13	37.70,−60.21, 181.77	36.53,−29.87, 137.57

Table 8 Femur position errors produced by the calculated 4R Spherical linkage (average error: 2.5mm)

% Stance Phase	**p** [mm]	**q** [mm]	**r** [mm]
0	0,0,0	0,0,0	0,0,0
25	0.05, 0.36, 1.25	0.03, 1.07, 0.97	0.19, 0.43, 1.02
50	0.52, 2.70, 0.36	0.29, 0.37, 0.14	0.36, 0.55, 0.13
75	1.62, 0.40, 3.67	1.64, 0.27, 2.64	0.30, 0.98, 2.82
100	5.77, 3.79, 13.45	5.69, 4.14, 11.81	4.35, 3.40, 12.38

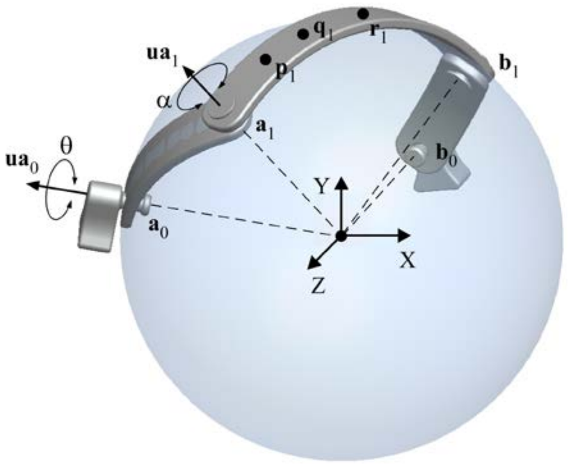

Fig. 9. 4R Spherical linkage dimensions and link displacement angles

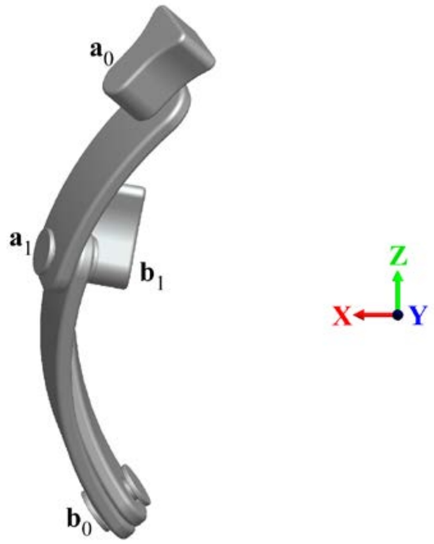

Fig. 10. Calculated 4R Spherical linkage

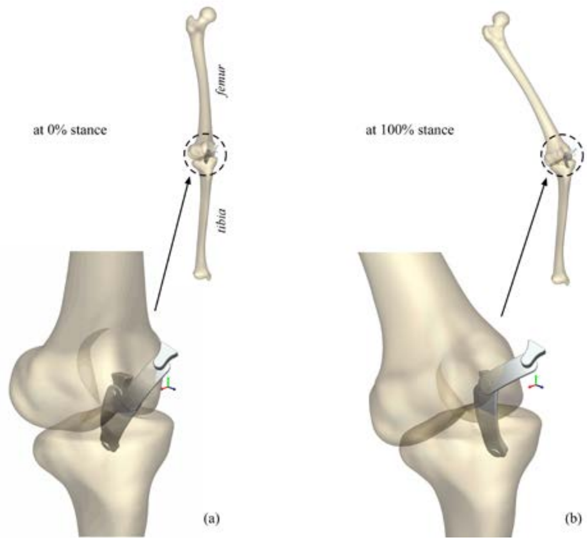

Fig. 11. Tibiofemoral motion with 4R Spherical linkage at (a) 0% stance and (b) 100% stance

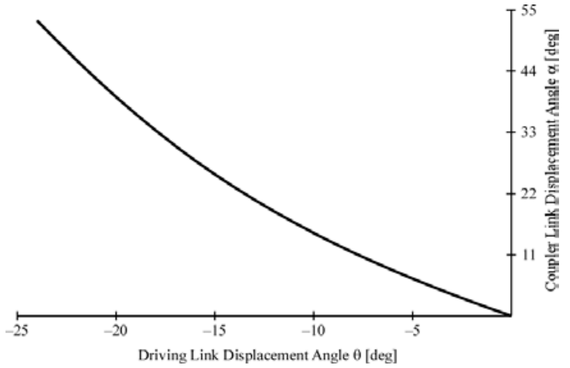

Fig. 12. 4R Spherical coupler angular displacement (α) versus crank angular displacement (θ) over given femoral motion range

DISCUSSION

While the examples in Section 3 only considered the five femoral positions in Table 2, the RRSS and 4R Spherical linkage optimization models can accommodate an indefinite number of prescribed positions (Russell and Shen 2013). As given in Tables 5 and 8, the average femur position errors for the calculated RRSS and 4R Spherical linkages are 1.1 and 2.5mm respectively. A larger error is produced by the 4R Spherical linkage because this linkage restricts the spatial motion of the femur to motion over a spherical surface. Since natural human tibiofemoral motion is not spherical, the femur position coordinates achieved by the calculated 4R Spherical linkage (Table 7) are more inaccurate than those produced by the RRSS linkage (Table 4). Therefore, the 4R Spherical linkage will be excluded from further discussion in this section. While the RRSS is the more accurate of the two linkages, even more accurate RRSS solutions than those in Tables 4 and 5 are possible by changing the initial values in Table 3 or the solution tolerances in the RRSS optimization model. The most accurate RRSS linkage however cannot achieve the zero error motion offered by the open-loop CCC linkage. On the other hand however, in a CAD-based mechanical modeling environment, the open-loop CCC linkage cannot achieve the ease of use (for CAD model development) offered by the RRSS linkage since the former requires the user to specify the motion of six parameters to control tibiofemoral motion. So the effectiveness of the RRSS linkage for knee motion analysis and simulation in a CAD-based mechanical modeling environment depends on the tibiofemoral position error allowable and the ease of use desired for CAD model development and operation. The error produced by the RRSS example (Table 5) is small enough to make the linkage suitable for a broad range tibiofemoral analyses and studies. The computer aided design and mechanical modeling software used in this work to implement the calculated RRSS and 4R Spherical linkage solutions for tibiofemoral motion (Figures 7 and 10) is *PTC Creo*.

CONCLUSION

Given 5 femur positions measured from an average human gait cycle, the calculated RRSS and 4R Spherical linkages produced average femur position errors of 1.1 and 2.5mm respectively. Because the motion of a 4R Spherical linkage is constrained to a spherical surface (and human tibiofemoral motion is not) this linkage cannot match the accuracy of the RRSS linkage. Neither linkage can match the zero error motion produced by an open-loop CCC linkage. The user has to specify the motion of six parameters to control tibiofemoral motion for the open-loop CCC linkage while the RRSS and 4R Spherical linkages only require the user to specify the motion of a single parameter. Having the user specify the motion of fewer parameters offers greater ease of use for model development and operation in a CAD-based mechanical modeling environment. The effectiveness of the RRSS and 4R Spherical linkages for knee motion analysis and simulation in a CAD-based mechanical modeling environment ultimately depends on the tibiofemoral position error allowable by the user and the ease of use desired by the user for CAD model development and operation.

REFERENCES

Belvedere C., Ensini A., Feliciangeli A., Cenni F., D'Angeli V., Giannini S. and Leardini A. 2012. Geometrical Changes of Knee Ligaments and Patellar Tendon During Passive Flexion. Journal of Biomechanics, 45(11): 1886-1892.

Benoit D. L., Ramsey D. K. , Lamontagne M., Xu L., Wretenberg P. and Renström P. 2007. In Vivo Knee Kinematics during Gait Reveals New Rotation Profiles and Smaller Translations. Clinical Orthopaedics and Related Research, 454(1): 81-88.

Dennis D. A., Mahfouz M. R., Komistek R. D. and Hoff W. 2005. In Vivo Determination of Normal and Anterior Cruciate Ligament-Deficient Knee Kinematics. Journal of Biomechanics, 38(2):241-253.

Gage J. R., Deluca P. A. and. Renshaw T. S, "Gait Analysis: Principles and Applications. 1995. Journal of Bone and Joint Surgery, 77(10):1607-1623.

Grood E. S. and Suntay W. J. 1983. A Joint Coordinate System for the Clinical Description of Three-dimensional Motions: Application to the Knee. Journal of Biomechanical Engineering, 105(2): 136-144.

Lee W. and Russell K. 2007. On Two-Phase Spherical Motion Generation. Journal of the Chinese Society of Mechanical Engineers, 28(6), 617-622.

Lee W. and Russell K. 2018. Developments in Quantitative Dimensional Synthesis (1970-Present): Four-Bar Motion Generation. Inverse Problems in Science and Engineering, 26(1) 133-148.

Russell K. and Shen Q. 2013. Expanded Spatial Four-Link Motion and Path Generation with Order and Branch Defect Elimination. Inverse Problems in Science and Engineering, 21(1):129–140.

空間和球形運動生成機構應用在膝關節運動分析與模擬的評估

李文宗
國立屏東科技大學生物機電工程系

摘 要

就機械觀點而言，通常使用開迴路式三圓柱對之空間連桿機構來描述人體膝蓋活動。該連桿最多具有 6 個自由度。雖然這種機構具有精確描述自然膝蓋運動的能力，但它需要使用者定義多達 6 個獨立的運動參數來實現它。相較之下，使用單個自由度可實現自然人體膝關節運動描述將有顯著進步性，因為使用者僅需定義單一個運動參數。在本研究中，評估空間機構雙旋轉-雙球面對(RRSS)和四旋轉對(4R)球面連桿（兩者都具單個自由度的空間四桿連）在人體膝關節運動分析與模擬的適用性。應用兩類連桿運動合成機構的優化模型以產生自然膝蓋運動的連桿尺寸。例如，計算雙旋轉-雙球面對(RRSS)和四旋轉對(4R) 球面連桿的尺寸，以在平均步行週期上實現一組脛骨-股骨位置。然後對這些連接進行建模，並在基於 CAD 的機械建模環境中模擬其運動。